

Electronic structure and bonding of small Pd clusters on stoichiometric and reduced SnO₂(110) surfaces



A. Robina^{a,b}, E. Germán^c, M.E. Pronsato^c, A. Juan^{c,*}, I. Matolínová^d, V. Matolín^d

^aFacultad de Ingeniería, Universidad Nacional de la Patagonia San Juan Bosco (UNPSJB), Ciudad Universitaria, 9500 Comodoro Rivadavia, Chubut, Argentina

^bDepartamento de Física, Universidad Nacional del Sur, Av. Alem 1253, 8000 Bahía Blanca, Argentina

^cDepartamento de Física, Universidad Nacional del Sur & IFISUR (UNS-CONICET), Av. Alem 1253, 8000 Bahía Blanca, Argentina

^dDepartment of Surface and Plasma Science, Faculty of Mathematics and Physics, Charles University in Prague, V Holešovičkách 2, 18000 Prague 8, Czech Republic

ARTICLE INFO

Article history:

Received 18 November 2013

Received in revised form

3 March 2014

Accepted 10 March 2014

Keywords:

Density functional theory

Palladium

SnO₂

Surface

Cluster

Adsorption

ABSTRACT

In the present work, we have studied the interaction of palladium adsorbed on SnO₂ (110) surfaces, considering the possible formation of clusters on the surface using density functional theory (DFT) calculations. We report structure, adsorption, and bonding properties of Pd_{*n*} (*n* = 1–5) on stoichiometric and reduced SnO₂ (110) surfaces. Although palladium can be adsorbed as metal clusters on both types of surfaces, these clusters can be more easily decomposed into Pd atoms on the reduced SnO₂ surface. Pd interacts mainly with bridging O atoms on stoichiometric surfaces while it bonds strongly with Sn on the reduced surface.

© 2014 Elsevier Ltd. All rights reserved.

1. Introduction

Metal oxide-based semiconductors such as SnO₂ have properties that make them interesting for several technological applications such as heterogeneous catalysts or gas sensors, since they present considerable surface reactivity with many reducing and oxidizing gases [1]. Tin oxide-based gas sensors operate on the principle of changes in surface conductivity when gas molecules interact with it [2–4]. Their sensing and catalytic properties like sensitivity, selectivity, operating temperature, etc, depend on grain size, texture, and stoichiometry and can be improved and/or optimized by adding small quantities of transition metals, like Pd, Pt, or Au [5–8]. However, reaction mechanisms on these systems are not well understood yet. The chemical properties of these small metal clusters formed on the surface are very different from those of the corresponding bulk systems and have a significant influence on catalytic reactions by supplying charges, adsorption sites, and new reaction paths.

Several experimental works have been devoted to the preparation and characterization of undoped and metal doped SnO₂ [9–

12]. Wang et al. employed a surfactant-mediated method to prepare SnO₂ nanocrystalline powders with a high surface area, thus obtaining nanoparticles with narrow particle distribution and an average 18.2 nm particle size. Vicent et al. studied the electrochemical behavior of antimony doped SnO₂ electrodes with and without platinum finding that the presence of Pt increases electrode stability. Sb doped SnO₂ was also studied by Szczuko et al. who analyzed the influence of different preparation techniques on dopant distribution and properties. They concluded that annealing temperature plays a major role in antimony distribution. The behavior of Os, Ni, Pd, and Pt doped SnO₂ was studied by Epifani et al. using thermal analysis and FTIR characterization. They observed that Pt and Pd, unlike Os and Ni, were likely to form nanoparticles in the SnO₂ lattice.

Previous research includes infrared studies performed on Pd/SnO₂ catalysts focused on the influence of pre-treatment on the species formed upon adsorption of CO and NO [13]. Gas sensing properties of Pd ultra-thin films deposited either on pyrolytically prepared SnO_{*x*} substrates or on SnO₂ powder were studied using X-ray photoelectron spectroscopy (XPS) and secondary ion mass spectroscopy (SIMS) [14,15]. It was demonstrated that reversible oxidation and reduction of Pd occurs during heating both in a normal and hydrogen containing atmosphere. SnO₂ supported Pd

* Corresponding author.

E-mail address: cajuan@uns.edu.ar (A. Juan).

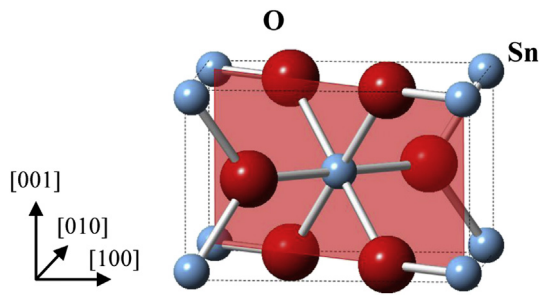


Fig. 1. Primitive cell of SnO_2 bulk structure. The shaded plane corresponds to the (110) surface.

particles were easier to oxidize and more difficult to reduce than a Pd(111) single crystal particle. This fact was attributed to the interaction between Pd particles and the SnO_2 substrate.

Pd particles supported on SnO_2 , using thin film and powder samples, have also been structurally studied by X-ray diffraction (XRD) and transmission and scanning electron microscopy (TEM & SEM) after different reductive treatments in order to monitor the eventual formation of bimetallic phases [16]. Formation of Pd_2Sn and PdSn at 573 K on the P/SnO_2 was observed on the thin film sample while Pd_3Sn_2 and Pd_2Sn were predominantly obtained on the powder catalyst.

Density Functional Theory (DFT) calculations have been employed in the past to predict SnO_2 system geometry, electronic structure, and energetics [17–20], and more recently, for the description of vibrational and optical properties [21,22]. In earlier DFT studies, Manassidis et al. used the pseudopotential method within the LDA approximation to calculate geometry and electronic distribution. Later, Rantala et al. employed the GGA approximation to describe the (110) surface band structure. Mäki-Jaskaari and Rantala have also calculated surface formation energies of oxygen-deficient SnO_2 (110) surfaces finding that the stoichiometric surface is the most stable and suggesting that stability decreases with increasing oxygen deficiency. Borges et al. calculated phonon frequencies, real and imaginary parts of complex dielectric function, energy loss spectrum, refractive index, extinction, and absorption coefficients that were in full agreement with experimental data. The optical properties calculated for tetragonal SnO_2 and SnO by Liu et al. explain the origin of spectral peaks and a significant optical anisotropy from polarization vectors (100) and (001) was demonstrated.

Petrova and Yakovkin studied the electronic structures of Sn and SnO_x layers adsorbed on the Pd(110) surface by DFT [23]. These authors found that the Sn 4d peak in photoemission spectra can serve as an unambiguous indicator of the degree of oxidation of Sn layers on transition metal surfaces.

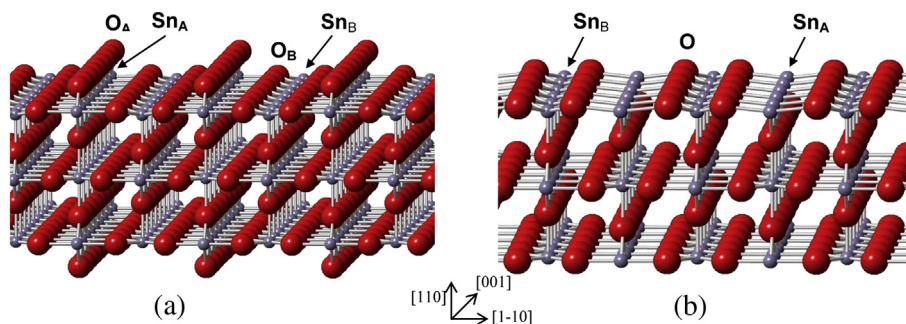


Fig. 2. (a) Stoichiometric $\text{SnO}_2(110)$ surface; atoms labeled Sn_A and Sn_B correspond to six-fold coordinated bulk-like tin atoms and five-fold coordinated tin surface atoms respectively. Atoms labeled O_A and O_B correspond to bridging oxygen atoms and to oxygen atoms bonded to both six-fold and five-fold coordinated Sn atoms. (b) Reduced $\text{SnO}_2(110)$ surface; atoms labeled Sn_A become four-fold coordinated and all oxygen atoms are labeled O.

DFT calculations have been performed for the interaction of CO with the undoped and Pd doped SnO_2 (110) surface. It was found that Pd doping can obviously enhance CO adsorption, which theoretically reproduces the experimental fact that Pd doping can greatly increase SnO_2 gas sensors' sensitivity to CO gas [24].

A first principles study showed that Pd/ SnO_2 (110) surface adsorbs more H_2 (gas) thus getting more electron density from the adsorbed molecule, thereby holding the potential for improvement of sensor response to hydrogen [25].

The energetics of several low-index SnO_2 surfaces has also been studied by DFT calculations, showing that the (110) surface is the one with the lowest surface energy [26,27].

The aim of this work is to study metal–substrate interaction in the Pd– SnO_2 system using DFT calculations. In order to do this, we begin by considering the most stable SnO_2 surface and adsorbing several Pd atoms. The possible formation of small Pd clusters on the SnO_2 substrate is considered for both stoichiometric and reduced (110) surfaces. Therefore, we report a study of adsorption geometries, energetics, electronic structure, and bonding of Pd_n ($n = 1–5$) clusters on $\text{SnO}_2(110)$ surfaces.

2. Computational method

DFT calculations were performed using the Vienna *Ab-Initio* Simulation Package (VASP) [28–31] which employs a plane-wave basis set and a periodic supercell method. Potentials within the projector augmented wave (PAW) method [32] and gradient-corrected functionals in the form of the generalized-gradient approximation (GGA) with Perdew–Burke–Ernzerhof (PBE) functional [33,34] were used.

For bulk optimization, SnO_2 lattice parameters were determined by minimizing the total energy of the unit cell using a conjugated-gradient algorithm to relax the ions [35]. The optimization of structural parameters was performed until the forces on atoms were less than 0.02 eV/\AA and all stress components were less than 0.001 eV/\AA^3 . A $5 \times 5 \times 5$ Monkhorst–Pack k-point grid for sampling the Brillouin zone was employed. The Brillouin zone was integrated using Monkhorst–Pack sets of k-points [36] (centered at the Γ point) depending on the supercell dimensions and on the number of atoms. Results for bulk relaxations were checked for convergence with respect to the number of k-points as well as energy cutoff and we chose a $5 \times 5 \times 5$ grid and 500 eV to ensure fully converging results. A large number of k-points were also considered but the change in the energies was less than 0.02%. The calculated lattice parameters obtained for bulk SnO_2 were $a = 4.81 \text{ \AA}$, $c = 3.22 \text{ \AA}$ which are a little higher than experimental values ($a = 4.74 \text{ \AA}$, $c = 3.19 \text{ \AA}$) [37]. Each lattice parameter was overestimated in 1.5–1.9%. The distance between two O or two Sn atoms was 3.25 \AA ,

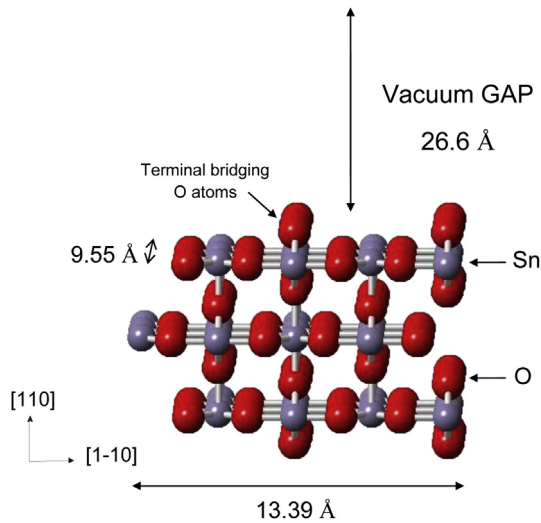


Fig. 3. SnO_2 (110) slab model built with 18 unit cells and a vacuum gap of 26.6 Å.

while the distance between Sn–O first neighbors was 2.10 Å. The computed value for the 219.6 GPa bulk modulus B was in full agreement with 218 GPa experimental data [38]. Parameter B was obtained by fitting the energy–volume data from minimization of energy at constant volumes to the Birch–Murnaghan equation of state [39,40].

The number of valence electrons considered for Sn, O, and Pd are 14, 6, and 10, respectively. The bulk rutile SnO_2 has a tetragonal structure with two SnO_2 units per unit cell. It is composed of six-fold coordinated Sn atoms and three-fold coordinated O atoms. Fig. 1 shows the unit cell where the (110) plane is also shown.

The SnO_2 (110) surface was modeled considering two different possible terminations. One of them is the stoichiometric surface (Fig. 2(a)) which contains bridging oxygen atoms keeping the composition of bulk SnO_2 . The second termination represents the fully reduced surface (Fig. 2(b)) where all bridging oxygen atoms were removed.

Table 1

Geometric parameters and overlap population (OP) for relevant bonds on the clean SnO_2 (110) surfaces and on SnO_2 with adsorbed Pd_n clusters ($n = 1, 5$).

SnO_2 (110)	Clean surface		Pd_1		Pd_5	
	Dist.(Å)	OP	Dist.(Å)	OP	Dist.(Å)	OP
Stoichiometric						
$\text{Sn}_A\text{--O}_A$	2.00	0.319	2.08	0.282	2.08	0.283
$\text{Sn}_A\text{--O}_B$	2.10	0.289	2.06	0.308	2.06	0.312
$\text{Sn}_B\text{--O}_B$	2.04	0.309	2.08	0.292	2.06	0.291
$\text{Sn}_A\text{--Sn}_A$	3.18	–	3.17	–	3.21	–
$\text{Sn}_B\text{--Sn}_B$	3.18	–	3.19	–	3.13	–
Pd--O_A			2.12	0.184	2.14	0.169
Pd--O_B			2.88	–	2.59 2.52	0.006
Pd--Sn_A			3.43	–	3.21	–
Pd--Sn_B			2.68	0.071	2.79–2.80	0.089
Pd--Pd^a					2.54–2.57	0.102–0.134
Reduced						
$\text{Sn}_A\text{--O}$	2.12	0.193	2.14	0.240	2.09	0.258
$\text{Sn}_B\text{--O}$	2.06	0.307	2.08	0.225	2.05	0.300
$\text{Sn}_A\text{--Sn}_A$	3.18	0.258	3.25	0.068	3.12	0.130
$\text{Sn}_B\text{--Sn}_B$	3.18	–	3.29	–	3.14	–
Pd--O			3.17	–	3.38	–
Pd--Sn_A			2.63	0.191	2.61	0.291
Pd--Sn_B			2.70	0.369	2.60	0.00
Pd--Pd^a					2.64–3.01	0.033–0.168
Sn–O distance (bulk): 2.10 Å						
Sn–Sn distance (bulk): 3.25 Å						

^a Length of Pd–Pd bonds in bulk fcc crystal 2.75 Å [40], in Pd_4 cluster 2.69 Å [52].

The stoichiometric surface presents two types of Sn atoms, six-fold coordinated bulk-like Sn atoms (labeled Sn_A in Fig. 2(a)) bonded to bridging oxygen atoms, and five-fold coordinated Sn atoms (labeled Sn_B in Fig. 2(a)). There are also two types of surface oxygen atoms, two-fold coordinated bridging O atoms (O_A in Fig. 2(a)), bonded to Sn_A and three-fold coordinated O atoms (O_B in Fig. 2(a)), bonded to both Sn_A and Sn_B . The reduced surface Sn_A atoms are now four-fold coordinated and all O atoms are equivalent.

The stoichiometric surface was modeled using a seven atom layer slab, three layers containing both Sn and O atoms, and six bridging O atom layers, as shown in Fig. 3. It was built up from 18

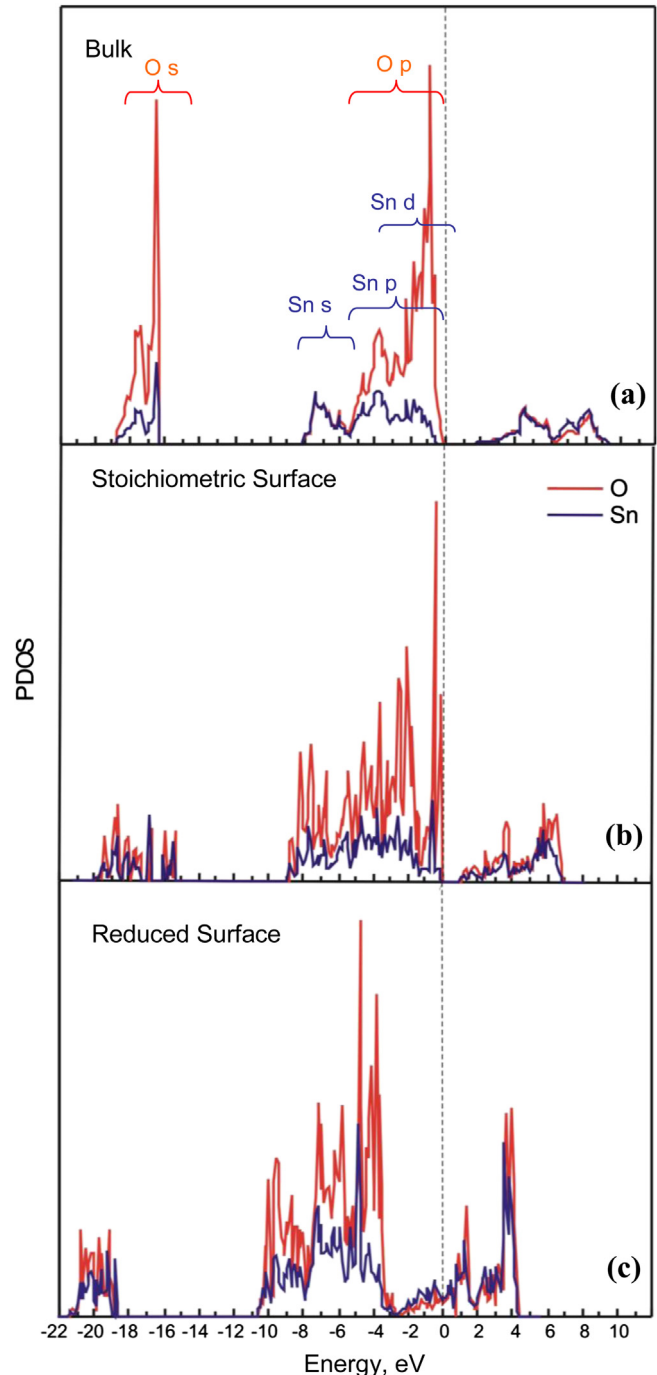


Fig. 4. PDOS of Sn and O for (a) bulk SnO_2 and for (b) the stoichiometric and (c) reduced SnO_2 (110) surfaces. The dashed line indicates the Fermi level.

unit cells, resulting in a supercell of 13.39 Å by 9.55 Å representing the surface with a thickness of 9.30 Å. The area of the surface is large enough to allow for the study of adsorbed species. The vacuum spacing between two repeated slabs was 26.6 Å. A thicker slab was also considered but no relevant differences in calculated surface energies were found. During optimization the first two layers were allowed to relax, and a set of $3 \times 3 \times 1$ Monkhorst–Pack k-points was used to sample the Brillouin zone. The same set of k-points was used by Xue and Tang and by Lin et al. on Pd and Ti doped SnO₂ (110) surfaces [24,41].

To model the reduced surface, we removed all terminal bridging oxygen atoms from the stoichiometric surface slab. In this case the slab had three layers containing Sn and O atoms and five bridging O atom layers.

The adsorption of Pd atoms on each type of the SnO₂ (110) surface and the possibility of cluster formation was studied. Preferential adsorption sites were found for one to five Pd atoms calculating their adsorption energies adding one atom at a time. During these calculations both the adsorbed species and the first two surface layers were allowed to relax. In all cases, cut-off energy was 500 eV.

Pd adsorption energy on the surface was computed by subtracting the energies of isolated gas phase Pd_n clusters and the clean surface from the energy of the adsorbed system as follows:

$$E_{\text{ads}} = E(\text{Pd}_n/\text{SnO}_2) - E(\text{Pd}_n) - E(\text{SnO}_2) \quad (1)$$

where $n = 1-5$ is the number of Pd atoms forming the cluster.

In this definition, negative adsorption energy corresponds to a stable adsorption on the surface. Spin polarized calculations were performed to obtain the energies of the gas phase Pd_n clusters which were calculated in a 20 Å cubic box at Γ point.

In order to evaluate the stability of growing Pd clusters on the surface, the sintering energy (E_s) can be calculated. We define E_s as

$$E_s = [E(\text{Pd}_{n-1}/\text{SnO}_2) + E(\text{Pd}_1/\text{SnO}_2)] - [E(\text{Pd}_n/\text{SnO}_2) + E(\text{SnO}_2)] \quad (2)$$

E_s is the energy needed to decompose a Pd_n cluster into a Pd_{n-1} cluster and a Pd monomer adsorbed on the surface.

Throughout this paper, two conceptual tools – density of states (DOS) and crystal orbital overlap population (COOP) curves – are used extensively to shed more light on the Pd–Sn–O interaction. The DOS curve is a plot of the number of orbitals per unit volume per unit energy. The COOP curve is a plot of the overlap population weighted DOS vs. energy. Integration of the COOP curve up to the Fermi level (E_f) gives the total overlap population of the bond specified. Looking at the COOP, we may analyze the extent to which specific states contribute to a bond between atoms or orbitals [42].

Our COOP calculations were performed using the tight-binding extended Hückel (EH) method [43–45], an approximate molecular orbital scheme, implemented with the Yet Another Extended Hückel Molecular Orbital Package (YAEHMOP) program [46], on DFT optimized geometries. A similar procedure, combining DFT and EH COOP's was performed by Papoian et al. [47].

3. Results and discussion

3.1. Surface characterization

A geometry optimization on both surfaces was performed allowing the top atom layers to fully relax while keeping the bottom layers at fixed positions maintaining their bulk lattice

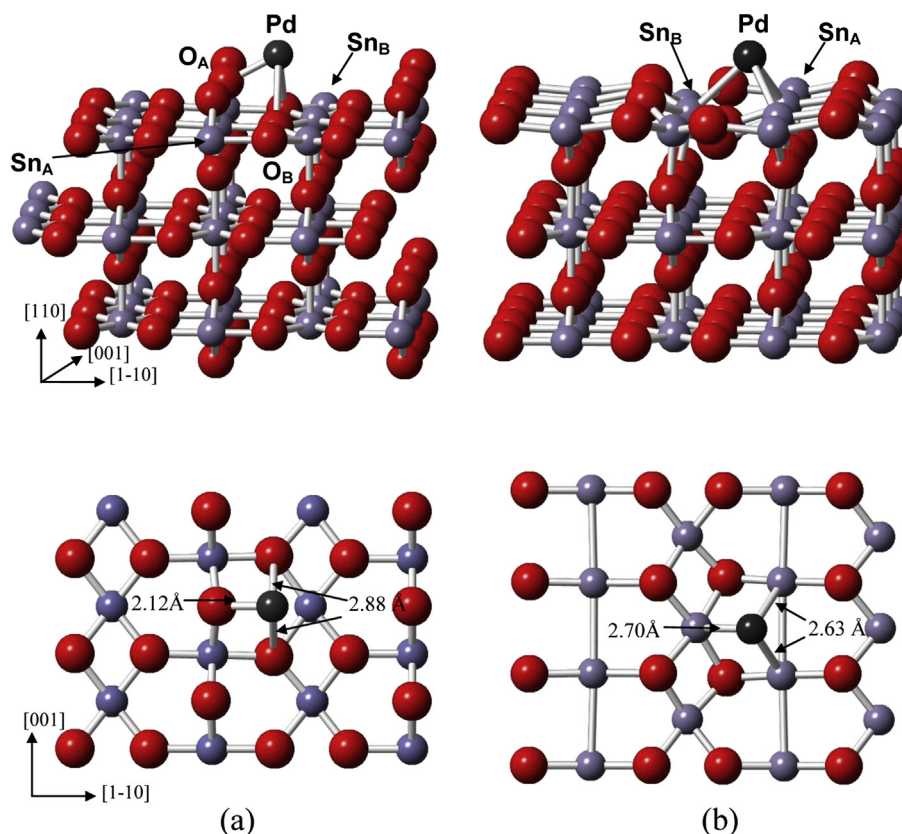


Fig. 5. Side and top view of the Pd adsorption site on the stoichiometric (a) and reduced (b) SnO₂ (110) surface.

parameters. A rearrangement of surface atoms occurs in order to minimize surface energy. The bond distance between Sn and surface O atoms is reduced between 2.8 and 4.6% with regard to bulk positions. The bond that contracts the most is the one between Sn_A and bridging O_A atoms which becomes 2.00 Å. In the case of the reduced surface, in which there is no O_A terminal bridging, the Sn_A –O bond distance increases slightly to 2.12 Å while the Sn_B –O distances decrease to 2.00 Å. Bond distances for bulk and surface atoms are summarized in Table 1, these results are in agreement with Oviedo et al. [48,49].

In order to analyze the electronic structure, projected DOS curves on surface atoms were plotted for both types of surfaces and were compared to bulk DOS curves (Fig. 4). SnO_2 is a material with a large band gap; its experimentally determined width is 3.6 eV [50]. The DOS plot for bulk SnO_2 shows the band gap of 2.3 eV width which is a smaller value than the one mentioned above. The dashed line indicates the Fermi level. The O 2s states are mainly located in the lower part of the valence band from –18.8 to –16.2 eV while most of the O 2p states extend through a broader region from –8 to 0 eV right below the Fermi energy, though there are also some unoccupied states. From the plot of the projected DOS on Sn atoms we may observe that most of Sn 4d states are occupied and that the conduction band is mainly composed of s and p states.

For the clean stoichiometric SnO_2 surface, PDOS curves on surface atoms show that the band gap is reduced to 1 eV. All the bands are shifted to lower energies; the O 2s states spread over a larger region at the bottom of the valence band from –20 to –15 eV and the O 2p states from –9 to 0 eV. There are also some states as part of the conduction band. The beginning of Sn bands also shifts about 1 eV to lower energies compared to the bulk SnO_2 and there are more unoccupied Sn d states.

The electronic structure for the reduced surface (see Fig. 4(c)) presents an important difference compared to the O terminated surface (Fig. 4(b)). PDOS plots show a shift of electronic states to lower energies in a way that no band gap is now observed indicating a metallic behavior. Both bands formed by O 2s states and O 2p are narrower than those observed for the stoichiometric surface. The surface is even more stabilized with O 2s states beginning at –21.2 up to –18.9 eV and the O 2p states form a band from –10.8 to 4.4 eV. This is due to the removal of the bridging O atoms from the surface.

3.2. Pd adsorption on $\text{SnO}_2(110)$ surfaces

In order to evaluate the interaction of adsorbed palladium and surface atoms, first we look for the preferential adsorption sites of Pd, placing one Pd atom in different positions on the surface and

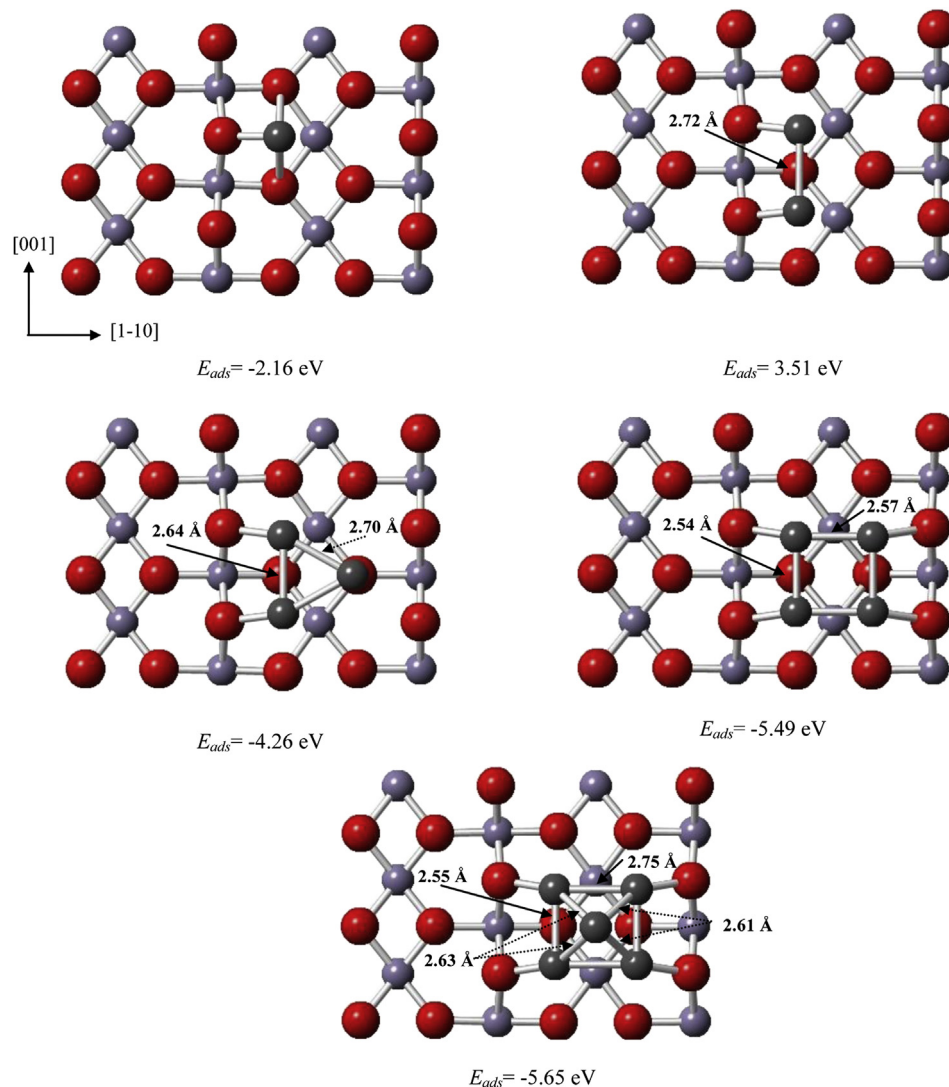


Fig. 6. Adsorption geometries of Pd_n cluster for $n = 1$ –5 on the stoichiometric $\text{SnO}_2(110)$ surface.

calculating the adsorption energy as previously defined. Table 1 summarizes the geometric parameters for Pd atoms on their most favorable adsorption sites for each type of surface.

For the stoichiometric surface, the minimum E_{ads} of -2.16 eV corresponds to the Pd located 2.12 Å from its first O_A neighbor and equidistant to two O_B , at 2.88 Å, as it can be seen in Fig 5(a).

On the reduced surface, the presence of Pd causes a major rearrangement of the surface layer compared to the oxygen terminated surface. Oxygen atoms are “pushed” away leaving the palladium atom closer to Sn atoms as shown in Fig. 5(b). A top-view shows how the palladium atom bonds to two Sn_A atoms with a bond length of 2.63 Å, and to one Sn_B , at 2.70 Å. In this case, the Pd that is nearer to the O neighbors is located at a distance of 3.17 Å which is a very different situation from the case of the stoichiometric surface. The distance between the two Sn_A atoms that bond to the palladium also increases, from 3.18 to 3.25 Å, as with bulk atoms. This new arrangement of atoms results in a stronger Pd–Sn interaction. The calculated adsorption energy at this site is -3.18 eV.

The interaction of the adsorbed Pd atoms with the substrate was also studied analyzing the overlap population (OP) between pairs of atoms before and after Pd adsorption.

For the stoichiometric surface, Pd interacts mainly with bridging O atoms. A Pd– O_A bond is formed affecting the bonding of its nearest neighbors. The OP between Sn_A and O_A near palladium decreases from 0.319 to 0.282 (around 12%), indicating a weakening of the Sn_A – O_A bond. The Sn_A – O_B overlap population increases a little, around 6.6% and Sn_B – O_B decreases 5.5%, due to the small shift in the position of O_B atoms towards Sn_A and away from Sn_B , so that the Pd– O_A bonds form mainly at the expense of the Sn_A – O_A bond. Finally, we noticed that the OP for the Pd– O_A bond is 0.184 while it is negligible between Pd and other oxygen atoms on the surface.

On the reduced surface the situation is different since Pd bonds to Sn surface atoms instead of O surface atoms. Sn_A – Sn_A bonds, which are strong on the clean surface, have an overlap population of 0.258 . When the palladium atom adsorbs on the surface, the OP between the two Sn_A atoms that bond to Pd decreases around 73%, to 0.068 . As a consequence, each Sn_A increases the strength of their bond with O and forms a strong bond with the adsorbed Pd atom (OP = 0.367). The palladium atom also bonds to its nearest Sn_B atom, with an overlap population of 0.191 , weakening the Sn_B –O bond. A summary of the OP between relevant bonds on the surfaces can be seen in Table 1.

The possibility of Pd cluster formation on the $SnO_2(110)$ surface was also studied by calculating the most stable adsorption sites for an increasing number of Pd atoms. After the preferential adsorption site for a single Pd atom was found, the most stable position for a second Pd atom was computed. Several possible sites were tested. The use of a big supercell to model the surface allowed us to test sites equivalent to the first adsorption site, both close to and far

from the first single Pd atom. For the stoichiometric surface, our calculations indicated that a second Pd atom will adsorb at an equivalent site as the previous one in its close proximity. Both Pd atoms remain at 2.12 Å from their first O_A neighbor and 2.72 Å from each other, which is close to the Pd–Pd distance in bulk fcc palladium (2.75 Å) [51]. The same procedure was followed for 3, 4, and 5 more Pd atoms until the final configuration of a small Pd cluster on the surface was obtained. Fig. 6 shows the adsorption geometries for Pd_n ($n = 1-5$) with the lowest adsorption energies. In the Pd_3 cluster, the third Pd atom bonds to the other two Pd atoms at a 2.70 Å distance while the remaining bond shortens to 2.64 Å. Pd–

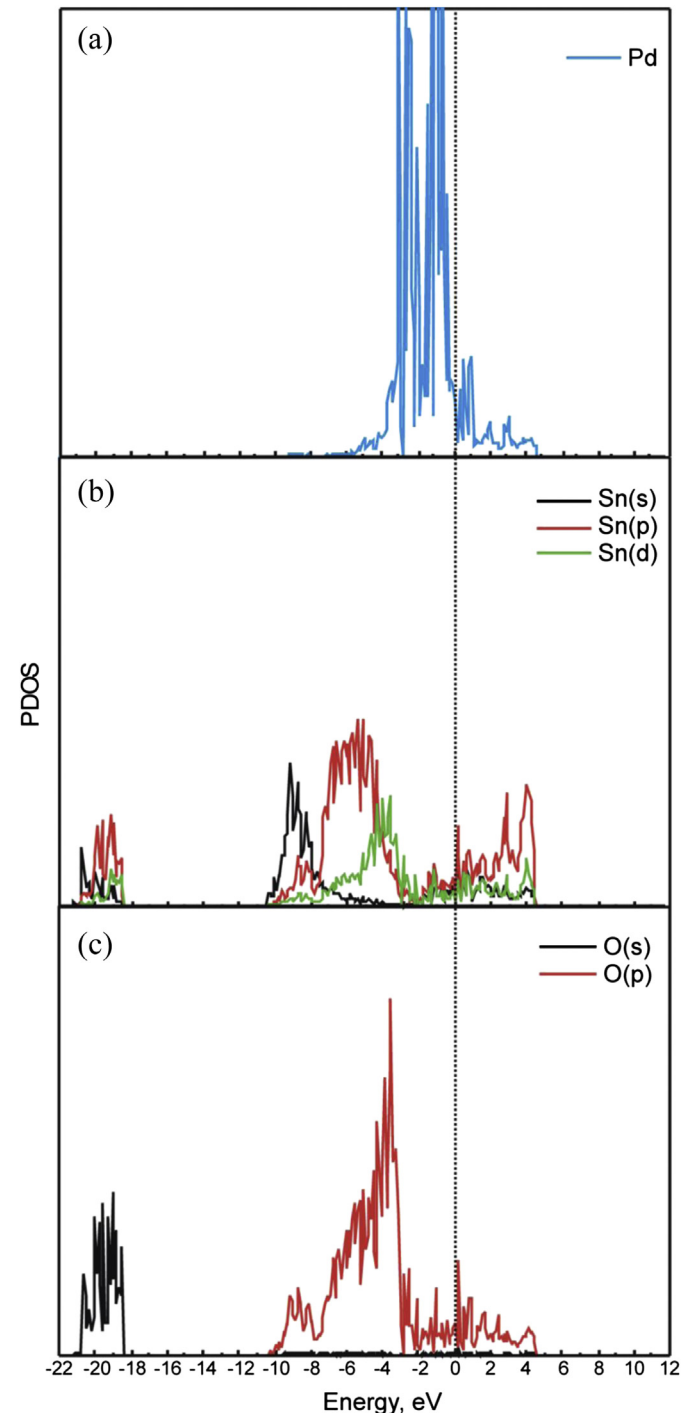


Fig. 7. PDOS on surface Sn (a), surface O (b) and Pd adsorbed (c) on stoichiometric $SnO_2(110)$ surface.

Table 2

Adsorption energy, E_{ads} , sintering energy E_s and Pd–Pd bond distances for Pd_n ($n = 1-5$) clusters adsorbed on the stoichiometric and reduced $SnO_2(110)$ surface.

	n	E_{ads} (eV)	E_s (eV)	Pd–Pd (Å)
Stoichiometric	1	-2.16	—	—
	2	-3.51	0.47	2.72
	3	-4.26	0.65	2.64–2.70
	4	-5.49	1.43	2.55–2.57
	5	-5.65	1.09	2.55–2.63
Reduced	1	-3.18	—	—
	2	-4.50	-0.58	2.88
	3	-6.12	0.50	2.71–2.83
	4	-6.04	-0.77	2.59–2.86
	5	-5.82	-0.32	2.64–3.01

Pd distances in the Pd₄ cluster are 2.55 Å and 2.53 Å, and for Pd₅ distances range from 2.55 to 2.75 Å.

Calculated adsorption and sintering energies are listed in Table 2. The positive sintering energy for each cluster indicates the energy cost of decomposing the Pd_n cluster into a monomer and a Pd_{n-1} cluster adsorbed on the surface. Therefore, it is better for stoichiometric surface Pds to be adsorbed as a cluster instead of as single atoms.

On the other hand, on the reduced surface, though clusters are stable as it can be observed by the negative adsorption energy, the

sintering energy is not always positive. So in this case the most favorable configuration would be Pd adsorbed on the surface as single atoms. The calculated distances between Pd atoms forming a cluster range and from 2.64 to 2.73 Å (see Table 1). The geometric details, E_{ads} and E_s for Pd_n cluster on the stoichiometric and reduced SnO₂(110) surface are summarized in Table 2.

The Pd–Pd overlap population for the stoichiometric surface ranges from 0.102 for the longest bond distance to 0.130 for the shortest bond. On the other hand, for the reduced surface OP varies between 0.033 and 0.168 showing a weaker bond strength between Pd atoms.

Figs. 7 and 8 show the projected PDOS curves on the surface and adsorbed atoms for the two types of surfaces. On the stoichiometric surface the plot shows some unoccupied Pd d states. The band extends from –5 to 6 eV. It can be seen that the main interaction with the surface is through O p states and some Sn d states. On the reduced surface, most of Pd d states lies below the Fermi level and O p states shift to lower energies. Therefore, the main interaction of Pd on the surface is with Sn d states in this case.

4. Conclusions

Pd adsorption on SnO₂ (110) was studied by DFT calculations. The band gap structure characteristic of SnO₂ is not present in the reduced surface due to a shift of electronic states to lower energies showing metallic behavior. Palladium can be adsorbed as metal clusters on both types of surfaces. These clusters can be easily decomposed into Pd atoms on the reduced SnO₂ (110) surface. Pd interacts mainly with bridging O atoms on the stoichiometric surfaces while it bonds strongly with Sn on the reduced surface. The main finding in our theoretical study is that stoichiometric surfaces should be used to assemble Pd/SnO₂ (110) gas sensors due to the presence of more stable Pd clusters on the surface that could improve H₂ gas adsorption and reactions.

Acknowledgments

The authors are grateful for the financial support from PICT-2010-1770, PICT-2012-1609, Res. 4541/12, MINCYT-MYES-ARC/13/11, SGCYT-UNS, CIC-Provincia Buenos Aires and grant 7AMB12AR004 from Czech Ministry of Education. E. Germán, A. Juan and M. E. Pronsato are members of CONICET. A. Robina acknowledges the support from Universidad Nacional de la Patagonia San Juan Bosco.

References

- [1] Batzill M, Diebold U. *Prog Surf Sci* 2005;79:47–154.
- [2] Göpel W, Schierbaum KD. *Sens Actuators B* 1995;26:1–12.
- [3] Ruhland B, Becker T, Muller G. *Sens Actuators B* 1998;50:85–94.
- [4] Ohnishi H, Sasaki H, Matsumoto T, Ippommatsu M. *Sens Actuators B* 1993;14:677–8.
- [5] Cabot A, Vilà A, Morante JR. *Sens Actuators B* 2002;84:12–20.
- [6] Chiorino A, Ghiotti G, Carotta MC, Martinelli G. *Sens Actuators B* 1998;47:205–12.
- [7] Li W, Shen C, Wu G, Ma Y, Gao Z, Xia X, et al. *J Phys Chem C* 2011;115:21258–63.
- [8] Kappler J, Barsan N, Weimar U, Dièguez A, Alay JL, Romano –Rodriguez A, et al. *Fresen J Anal Chem* 1998;361:110–4.
- [9] Wang Y-D, Ma Ch-L, Sun X-D, Li H-D. *Nanotechnology* 2002;13:565–9.
- [10] Vicent F, Morallón E, Quijada C, Vázquez JL, Aldaz A, Cases F. *J Appl Electrochem* 1998;28:607–12.
- [11] Szczuko D, Werner J, Behr G, Oswald S, Wetzig K. *Surf Interface Anal* 2001;31:484–91.
- [12] Epifani M, Alvisi M, Mirengi L, Leo G, Siciliano P, Vasanelli L. *J Am Ceram Soc* 2001;84(1):48–54.
- [13] Amalric-Popescu D, Bozon-Verduraz F. *Catal Today* 2001;70:139–54.
- [14] Skála T, Veltruská K, Moroseac M, Matolínová I, Cirera A, Matolín V. *Surf Sci* 2004;566–568:1217–21.

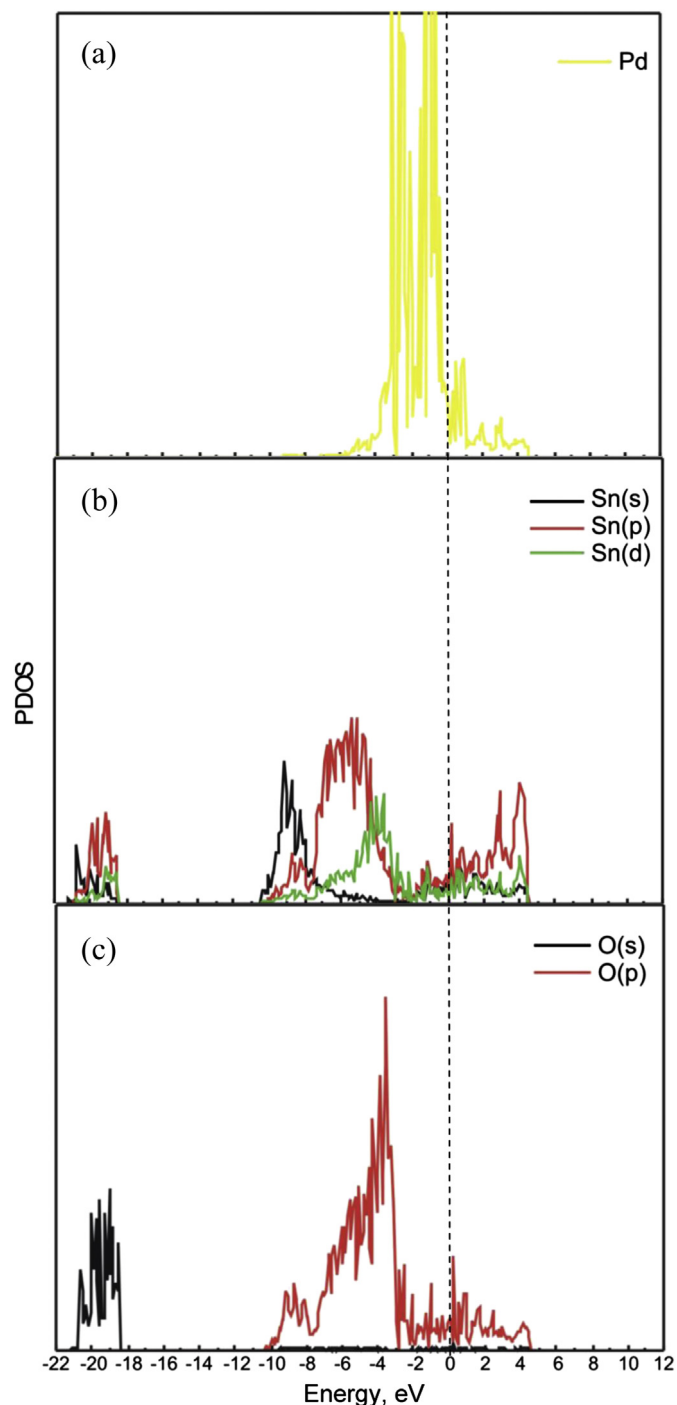


Fig. 8. PDOS on surface Sn (a), surface O (b) and Pd adsorbed (c) on reduced SnO₂ (110) surface.

- [15] Moroseac M, Skála T, Veltruská K, Matolín V, Matolínová I. *Surf Sci* 2004;566–568:1118–23.
- [16] Lorenz H, Zhao Q, Turner S, Lebedev OI, Van Tendeloo G, Klötzer B, et al. *Appl Catal A Gen* 2010;381:242–52.
- [17] Manassidis I, Gonniakowski J, Kantorovich LN, Gillan MJ. *Surf Sci* 1995;339:258–71.
- [18] Rantala TT, Rantala TS, Lantto V. *Mat Sci Sem Proc* 2000;3:103–7.
- [19] Mäki-Jaskari MA, Rantala TT. *Phys Rev B* 2002;65:245428 1–8.
- [20] Mäki-Jaskari MA, Rantala TT. *Surf Sci* 2003;537:168–78.
- [21] Borges PD, Scolfaro LMR, Leite Alves HW, da Silva Jr ER. *Theor Chem Acc* 2010;126:39–44.
- [22] Liu W, Liu Z, Feng L. *Comput Mat Sci* 2010;47:1016–22.
- [23] Petrova NV, Yakovkina IN. *Eur Phys J B* 2013;86:303–7.
- [24] Xue YB, Tang ZA. *Sens Actuators B* 2009;138:108–12.
- [25] Zeng W, Liu T, Liu D, Han E. *Sens Actuators B* 2011;160:455–62.
- [26] Oviedo J, Gillan MJ. *Surf Sci* 2000;463:93–101.
- [27] Prades JD, Cirera A, Morante JR, Runeda JM, Ordejón P. *Sens Actuators B* 2007;126:62–7.
- [28] Kresse G, Hafner J. *Phys Rev B* 1993;47:558–61.
- [29] Kresse G, Hafner J. *Phys Rev B* 1994;49:14251–69.
- [30] Kresse G, Furthmüller J. *Comput Mater Sci* 1996;6:15–50.
- [31] Kresse G, Furthmüller J. *Phys Rev B* 1996;54:11169–86.
- [32] Kresse G, Joubert J. *Phys Rev B* 1999;59:1758–1755.
- [33] Perdew JP, Burke K, Ernzerhof M. *Phys Rev Lett* 1996;77:3865–8.
- [34] Perdew JP, Burke K, Ernzerhof M. *Phys Rev Lett* 1997;78:1396–1396.
- [35] Press WH, Flannery BP, Teukolsky SA, Vetterling WT. *Numerical recipes*. New York: Cambridge University Press; 1986.
- [36] Monkhorst HJ, Pack JD. *Phys Rev B* 1976;13:5188–92.
- [37] Bolzan AA, Fong C, Kennedy BJ, Howard CJ. *Acta Crystallogr Sect B – Struct Sci* 1997;53:373–80.
- [38] Hazen RM, Finger LW. *J Phys Chem Solids* 1981;42:143–51.
- [39] Birch F. *J Appl Phys* 1938;9:279–88.
- [40] Birch F. *Phys Rev* 1947;71:809–24.
- [41] Lin W, Zhang W-F, Li Y, Ding K-N, Li J-Q, Xu Y-J. *J Chem Phys* 2006;124:054704 1–8.
- [42] Hoffmann R. *Solids and surfaces: a chemist's view of bonding in extended structures*. New York: VCH; 1988.
- [43] Hoffmann R, Lipscom WN. *J Chem Phys* 1962;36:2179–89.
- [44] Hoffmann R. *J Chem Phys* 1963;39:1397–412.
- [45] Whangbo M-H, Hoffmann R. *J Am Chem Soc* 1978;100:6093–8.
- [46] Landrum G, Glassey W. *Yet another extended Hückel molecular orbital package (YAeHMOP)*. New York: Cornell University; 1997. <http://yaehmop.sourceforge.net>.
- [47] Papoian G, Norskov JK, Hoffmann R. *J Am Chem Soc* 2000;122:4129–44.
- [48] Oviedo J, Gillan MJ. *Surf Sci* 2002;513:26–36.
- [49] Oviedo J, Gillan MJ. *Surf Sci* 2001;490:221–36.
- [50] Dawar AL, Joshi JC. *J Mater Sci* 1984;19:1–23.
- [51] Kittel C. *Introduction to solid state physics*. John Wiley & Sons; 2005.
- [52] Zhang J, Alexandrova AN. *J Chem Phys* 2011;135:174702/1–174702/10.